BUTTERWORTH HEINEMANN

Momentum and thermal boundary layer along a slender cylinder in axial flow

E. Richelle, R. Tasse and M. L. Riethmuller
von Karman Institute for Fluid Dynamics, Rhode-Saint-Genèse, Belgium

A laminar approach of the melt-spinning process is presented, using nondimensionalized momentum and thermal boundary-layer equations. The momentum boundary layer along a yarn of circular cross section in axial flow is investigated for two types of boundary conditions; the quasi-similar solution is computed for both a semi-infinite body and a continuous moving surface, using a finite difference scheme. The comparison exhibits a difference between the growth of the boundary layer in the two cases. The quasi-similar solution is extended to the thermal boundary layer along a moving yarn. The computation is carried out in the air as well as inside the yarn, yielding the temperatures, the Nusselt number, and boundary-layer thickness as functions of a dimensionless parameter.

Keywords: axial flow; axisymmetric flows; boundary layers; cylinder; heat transfer

Introduction

The melt-spinning process consists of extruding a molten polymer from an array of holes in a spinneret. The yarns that are created are cooled down by their motion in the air and by a lateral quenching air flux, while their diameter decreases because of the stretching provided by the rotating bobbin, until they solidify.

The objective of this paper is to provide the laminar solution of this problem, for both the velocities and the temperatures in the vicinity of the yarn. The lateral air flux is not taken into account, and the cross section of the yarn is assumed to be a circle of constant diameter.

The laminar boundary layer along a circular cylinder has been investigated by many authors, since Seban and Bond (1951). Sakiadis (1961a, 1961b, 1961c) has shown the difference between the boundary conditions encountered by a continuous moving surface in a fluid at rest, and by a semi-infinite body mounted in a wind tunnel. The boundary layer is initialized by the spinneret in the first case (spinneret case); whereas it grows from the body leading edge in the latter case (wind-tunnel case), as illustrated in Figures 1 and 2, respectively. Sakiadis has computed the solution of Blasius' equation in both cases, showing that inverting the boundary conditions does not lead to an exactly inverted velocity profile.

As found by Seban and Bond (1951) and later by Glauert and Lighthill (1955), Jaffe and Okamura (1968), Kao and Chow (1991), and Sawchuk and Zamir (1992), the laminar momentum boundary-layer equations can be nondimensionalized by using a transformation of coordinate system. Sawchuk and Zamir have computed the solution for the wind-tunnel case, in a large range of the dimensionless parameters.

The present paper investigates the laminar boundary layer for both the wind-tunnel and the spinneret cases. The computation of the axisymmetric boundary layer is performed first for the wind-tunnel case. The flowfield obtained in this paper is compared with Sawchuk's and Zamir's results. Then the spinneret case is considered. The boundary-layer equations are solved using a finite difference method, and the results are compared to the previous wind-tunnel computation, showing significant differences.

The transformation of coordinate system for the momentum computation is extended to the thermal boundary-layer equations. Because the surface temperature along the yarn is unknown, the computation is also performed inside the yarn. The results of the laminar axisymmetric thermal boundary-layer computation along a continuous moving body are presented as functions of dimensionless parameters, and could be used for many engineering applications.

Momentum boundary-layer equations

The moving thread is modeled as a cylinder of contrast radius a. The origin of the x, r coordinate system is located in the center of the leading-edge cross section of the yarn (wind-tunnel case) or in the center of the spinneret hole (spinneret case). The

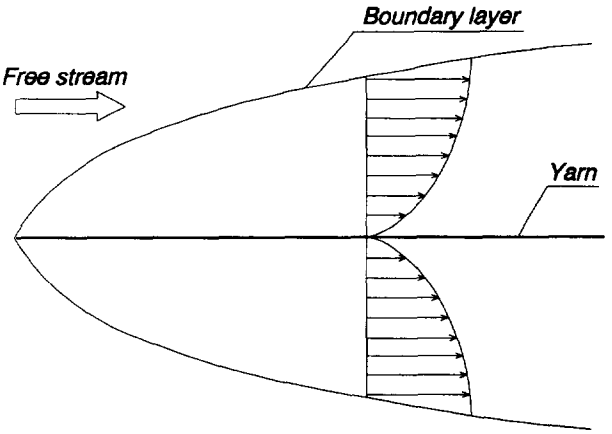

Figure 1 The wind-tunnel case

Address reprint requests to Prof. M. L. Riethmuller, von Karman Inst. for Fluid Dynamics, Chaussée de Waterloo, 72, 1640 Rhode-Saint-Genèse, Belgium.

Received 14 September 1993; accepted 2 October 1994

Int. J. Heat and Fluid Flow 16: 99–105, 1995

655 Avenue of the Americas, New York, NY 10010

SSDI 0142-727X/95/$10.00
SSDI 0142-727X(94)00012-2

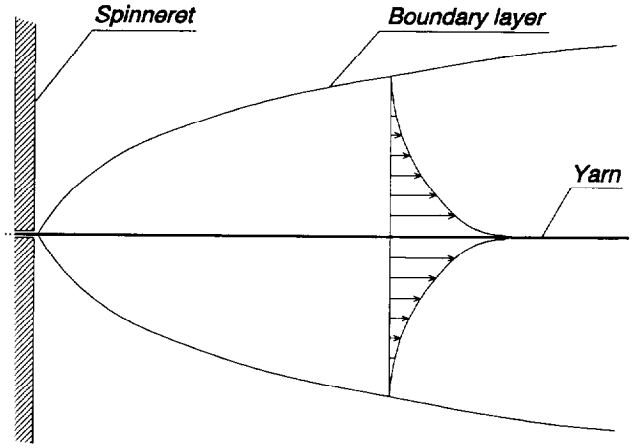

Figure 2 The spinneret case

x-axis is the symmetry axis; whereas, the y-coordinate is measured in the radial direction from the yarn surface. The laminar velocity field is governed by the following two-dimensional (2-D) boundary-layer equations

$$\frac{\partial u}{\partial x} + \frac{v}{a+y} + \frac{\partial v}{\partial y} = 0 \tag{1}$$

$$u\frac{\partial u}{\partial x} + v\frac{\partial u}{\partial y} = -\frac{1}{\rho}\frac{\partial p}{\partial x} + \nu\left(\frac{1}{a+y}\frac{\partial u}{\partial y} + \frac{\partial^2 u}{\partial y^2}\right) \tag{2}$$

$$\frac{\partial p}{\partial y} = 0 \tag{3}$$

The boundary layer conditions are the velocities at the wall and at infinity. For the wind-tunnel case they are as follows:

$$\begin{aligned} u &= 0 \quad \text{at} \quad y = 0 \\ v &= 0 \quad \text{at} \quad y = 0 \\ u &= u_e \quad \text{at} \quad y = \infty \end{aligned} \tag{4}$$

Notation

a yarn radius
A parameter used for the mesh generation, Equation 39
Br Brinkman number
c parameter governing the stretching intensity in Equation 37
C_f friction coefficient
c_p specific heat capacity
Ec Eckert number
f dimensionless stream function
k heat conduction coefficient
L typical streamwise length
Nu_a Nusselt number based on a
Nu_x Nusselt number based on x
p pressure
Pr Prandtl number
r radial coordinate, origin on the symmetry axis
St Stanton number
Re_a Reynolds number based on a
Re_x Reynolds number based on x
T local temperature
T_0 $(\partial u/\partial \eta)_{\eta=0}$
T_e free-stream temperature
T_{wo} temperature of the yarn at the exit of the spinneret
u axial velocity
u_e free-stream velocity (wind-tunnel case), yarn velocity (spinneret case)
U_{inf} dimensionless free-stream velocity
U_{wall} dimensionless wall velocity
v radial velocity
x axial coordinate along the yarn
y radial coordinate, origin at the yarn surface
z argument of mesh generation functions

Greek

α thermal diffusivity
α_m parameter governing the stretching center in Equation 38
β_m parameter governing the stretching intensity in Equation 38
δ boundary-layer thickness
δ_T thermal boundary-layer thickness
δ^* boundary-layer displacement thickness
Wind-tunnel case:

$$\pi(\delta^* + a)^2 - \pi a^2 = \int_a^\infty (1 - u/u_e)2\pi r \, \mathrm{d}r$$

Spinneret case:

$$\pi(\delta^* + a)^2 - \pi a^2 = \int_a^\infty u/u_e 2\pi r \, \mathrm{d}r$$

δ_T^* thermal boundary-layer displacement thickness
Spinneret case only:

$$\pi(\delta_T^* + a)^2 - \pi a^2 = \int_0^\infty u/u_e \cdot (T - T_{wo})/(T_e - T_{wo})2\pi r \, \mathrm{d}r$$

η dimensionless number defined as $y\sqrt{u_e/2\nu x}$
θ boundary-layer momentum thickness
Wind tunnel case:

$$\pi(\theta + a)^2 - \pi a^2 = \int_a^\infty u/u_e(1 - u/u_e)2\pi r \, \mathrm{d}r$$

Spinneret case:

$$\pi(\theta + a)^2 - \pi a^2 = \int_a^\infty u/u_e \, u/u_e \, 2\pi r \, \mathrm{d}r$$

Θ dimensionless temperature
μ dynamic viscosity
ν kinematic viscosity
ξ dimensionless number $\sqrt{\nu x/u_e a^2}$
ρ mass per unit volume
ϕ_1 $(u_e/\nu a^2 x)^{1/2} \int_a^\infty (1 - u/u_e) r \, \mathrm{d}r$
ϕ_2 $(u_e/\nu a^2 x)^{1/2} \int_a^\infty u/u_e(1 - u/u_e) r \, \mathrm{d}r$
ψ stream function

Subscript

s subscript, Referring to the yarn (solid)

and for the spinneret case

$$\begin{aligned} u &= u_e \quad \text{at} \quad y = 0 \\ v &= 0 \quad \text{at} \quad y = 0 \\ u &= 0 \quad \text{at} \quad y = \infty \end{aligned} \tag{5}$$

These equations are nondimensionalized using a transformation from x, y to ξ, η. The definition of ξ and η is not unique, as shown by the previous works performed on the subject, by Jaffe and Okamura (1968), Kao and Chow (1991), and Sawchuk and Zamir (1992). For an easy comparison with Sawchuk and Zamir, the following choice has been made:

$$\begin{cases} \eta = y\sqrt{\dfrac{u_e}{2\nu x}} \\ \xi = \sqrt{\dfrac{x\nu}{u_e a^2}} \end{cases} \Leftrightarrow \begin{cases} y = a\sqrt{2}\xi\eta \\ x = \xi^2 \dfrac{u_e a^2}{\nu} \end{cases} \tag{6}$$

The continuity equation is identically satisfied by using the stream-function approach.

$$u = \frac{1}{a+y}\partial_y\psi \quad \text{and} \quad v = -\frac{1}{a+y}\partial_x\psi$$

where ψ is nondimensionalized as $f = \psi/a\sqrt{u_e \nu x}$.

Assuming that the free-stream velocity is constant ($\partial_x p = 0$) leads to the final equation:

$$\begin{aligned} f_{\eta\eta\eta} = {} & f_{\eta\eta}\cdot(2\xi - f - \xi f_\xi)/\sqrt{2}(1 + \xi\eta\sqrt{2}) \\ & + \xi f_\eta/\sqrt{2}(1 + \xi\eta\sqrt{2})^2 \\ & \times [(1 + \xi\eta\sqrt{2})f_{\eta\xi} - \eta\sqrt{2}f_\eta \\ & + \xi\sqrt{2}f_\xi + \sqrt{2}f - 2\sqrt{2}\xi] \end{aligned} \tag{7}$$

with the following boundary conditions:

$$\begin{aligned} & f = 0 \text{ for } \eta = 0;\ (f_\eta/\sqrt{2}) = U_{\text{wall}} \text{ at the wall } \eta = 0; \\ & \text{and } (f_\eta/\sqrt{2}(1 + \xi\eta\sqrt{2}) = U_{\text{inf}} \text{ at infinity } \eta = \infty. \end{aligned} \tag{8}$$

where the dimensionless boundary velocities ($U_{\text{wall}}, U_{\text{inf}}$) are 0, 1 for the wind-tunnel case and 1, 0 for the spinneret case. The first boundary condition in Equation 8 is given by the zero transverse velocity at the wall. In the case of a flat plate $a = \infty$, $\xi = 0$ and Equation 7 reduces to the Blasius equation:

$$f_{\eta\eta\eta} + f\cdot f_{\eta\eta} = 0 \tag{9}$$

The solution of this equation is then used as an initial condition for Equation 7.

As in the case of a flat plate, the velocities, the boundary-layer thicknesses, and the friction coefficient can be determined from the knowledge of f. The velocity components are given as functions of f by the following:

$$\begin{aligned} & u/u_e = 1/\sqrt{2}\cdot 1/(1 + \xi\eta\sqrt{2})\cdot f_\eta \\ & \text{and} \\ & v/u_e\cdot\sqrt{\text{Re}_x} = 1/2\cdot 1/(1 + \xi\eta\sqrt{2})\cdot(\eta f_\eta - \xi f_\xi - f) \end{aligned} \tag{10}$$

Substitution of the velocity in the axisymmetric definition of δ^* leads to the following relationships.

For the wind-tunnel case:

$$\pi(\delta^* + a)^2 - \pi a^2 = \int_a^\infty \left(1 - \frac{u}{u_e}\right)2\pi r\, dr \tag{11}$$

$$(\delta^*/a + 1)^2 - 1 = 2\xi(\eta\sqrt{2} + \xi\eta^2 - f)_{(\eta=\infty)} \tag{12}$$

For the spinneret case:

$$\pi(\delta^* + a)^2 - \pi a^2 = \int_a^\infty \frac{u}{u_e} 2\pi r\, dr \tag{13}$$

$$(\delta^*/a + 1)^2 - 1 = 2\xi f_{(\eta=\infty)} \tag{14}$$

A similar calculation performed for the momentum boundary-layer thickness gives the following:

$$\pi(\theta + a)^2 - \pi a^2 = \int_a^\infty \frac{u}{u_e}\left(1 - \frac{u}{u_e}\right)2\pi r\, dr \tag{15}$$

$$\left(\frac{\theta}{a} + 1\right)^2 - 1 = 2\xi\left(f_{(\eta=\infty)} - \frac{1}{\sqrt{2}}\int_0^\infty \frac{f_\eta^2}{1 + \xi\eta\sqrt{2}}\, d\eta\right) \tag{16}$$

for the wind-tunnel case, and

$$\pi(\theta + a)^2 - \pi a^2 = \int_a^\infty \frac{u}{u_e}\frac{u}{u_e} 2\pi r\, dr \tag{17}$$

$$\left(\frac{\theta}{a} + 1\right)^2 - 1 = 2\xi\frac{1}{\sqrt{2}}\int_0^\infty \frac{f_\eta^2}{1 + \xi\eta\sqrt{2}}\, d\eta \tag{18}$$

for the spinneret case. The friction coefficient, defined for both cases as follows:

$$C_f = \frac{\mu\left.\dfrac{\partial u}{\partial y}\right|_{y=0}}{\frac{1}{2}\rho u_e^2} \tag{19}$$

is given by the following:

$$C_f\cdot\sqrt{\text{Re}_x} = (f_{\eta\eta} - \xi\sqrt{2}f_\eta)_{(\eta=0)} \tag{20}$$

The thermal problem

The velocity field has been derived for both the wind-tunnel and the spinneret cases, using two dimensionless parameters ξ and η. Because the fiber-spinning process involves heat transfer aspects, the thermal boundary layer has also been investigated for the spinneret case. In the axisymmetrical case, the boundary-layer approximation applied to the energy equation yields the following equation:

$$\begin{aligned} u\frac{\partial T}{\partial x} + v\frac{\partial T}{\partial y} = {} & \frac{k}{\rho c_p}\left(\frac{1}{a+y}\frac{\partial T}{\partial y} + \frac{\partial^2 T}{\partial y^2}\right) \\ & \underbrace{+ 2\frac{\nu}{c_p}\left\{\left(\frac{\partial v}{\partial y}\right)^2 + \left(\frac{v}{a+y}\right)^2 + \left(\frac{\partial u}{\partial x}\right)^2\right\}}_{(a)} \\ & \underbrace{+ \frac{\nu}{c_p}\left\{\frac{\partial u}{\partial y}\right\}^2}_{(b)} \end{aligned} \tag{21}$$

The viscous dissipation terms, (*a*) and (*b*), can be neglected because they are of the order of $\text{Ec}/\text{Re}_L \approx 10^{-9}$ and $\text{Br} \approx 10^{-4}$. The thermal boundary-layer equation reduces to the following:

$$u\frac{\partial T}{\partial x} + v\frac{\partial T}{\partial y} = \frac{k}{\rho c_p}\left(\frac{1}{a+y}\frac{\partial T}{\partial y} + \frac{\partial^2 T}{\partial y^2}\right) \tag{22}$$

Substituting x, y to ξ, η in Equation 22, and introducing the reduced temperature Θ defined as $\Theta = T - T_e/(T_{wo} - T_e)$ with T the local temperature; T_{wo} the temperature of the yarn at the exit of the spinneret; and

T_∞, the air temperature at infinity leads to the following:

$$\Theta_{\eta\eta} + \xi\sqrt{2}/(1 + \xi\eta\sqrt{2})\cdot\Theta_\eta = \nu/\alpha/\sqrt{2}\cdot 1/(1 + \xi\eta\sqrt{2})\cdot(\xi\Theta_\xi f_\eta - \xi\Theta_\eta f_\xi - \Theta_\eta f) \tag{23}$$

$\alpha = k/\rho c_p$ is the thermal diffusivity of the fluid. This parabolic equation requires one initial condition and two boundary conditions. As in the case of the momentum Equation 7, at $\xi = 0$ the equation reduces to an ordinary differential equation. The solution of this equation provides the initial condition for Equation 23. One external boundary condition and two jump conditions are needed. The external boundary condition is given by the following:

$$T_{(y=\infty)} = T_e \quad \text{at} \quad y = \infty \tag{24}$$

while the jump conditions at the interface are as follows:

$$T_{\text{air}} = T_{\text{yarn}} \quad \text{at} \quad y = 0 \tag{25}$$

$$k_{\text{air}}\frac{\partial T_{\text{air}}}{\partial y} = k_{\text{yarn}}\frac{\partial T_{\text{yarn}}}{\partial y} \quad \text{at} \quad y = 0 \tag{26}$$

The jump conditions show that the yarn itself has to be included in the computation domain. The yarn is assumed to be a solid of constant diameter moving at a constant velocity. The temperature distribution inside it is governed by the following equation:

$$\rho_s c_{p,s} u_e \frac{\partial T}{\partial x} = k_s\left(\frac{\partial^2 T}{\partial y^2} + \frac{1}{r}\frac{\partial T}{\partial y} + \frac{\partial^2 T}{\partial x^2}\right) \tag{27}$$

where the subscript s means *solid*. Inserting ξ and η in the simplified equation leads to the following:

$$\Theta_{\eta\eta} + \xi\sqrt{2}/(1 + \xi\eta\sqrt{2})\cdot\Theta_\eta = \nu/\alpha_s\cdot(-\eta\Theta_\eta + \xi\Theta_\xi) \tag{28}$$

The first boundary condition is the yarn temperature at the exit of spinneret; i.e., the melting temperature $T = T_{wo}$ and the second boundary condition is the symmetry condition

$$\left.\frac{\partial T}{\partial r}\right|_{r=0} = 0$$

The nondimensionalized thermal equations in the air and in the cylinder have been derived as well as the boundary conditions at the edges of the computation domain. They are summarized in their dimensionless form as follows:

$$\Theta_{\eta\eta} + \xi\sqrt{2}/(1 + \xi\eta\sqrt{2})\cdot\Theta_\eta = \nu/\alpha/\sqrt{2}\cdot 1/(1 + \xi\eta\sqrt{2})\cdot(\xi\Theta_\xi f_\eta - \xi\Theta_\eta f_\xi - \Theta_\eta f) \quad \text{for} \quad \eta > 0 \tag{29a}$$

$$\Theta_{\eta\eta} + \xi\sqrt{2}/(1 + \xi\eta\sqrt{2})\cdot\Theta_\eta = \nu/\alpha_s\cdot(-\eta\Theta_\eta + \xi\Theta_\xi) \quad \text{for} \quad \eta < 0 \tag{29b}$$

with the following boundary conditions

$$\Theta = 1 \quad \text{at} \quad \xi = 0,\ \eta = -\infty \tag{30a}$$

$$\Theta = 0 \quad \text{at} \quad \xi \geq 0,\ \eta = \infty \tag{30b}$$

$$\Theta(\eta = 0^-) = \Theta(\eta = 0^+) \quad \text{at} \quad \eta = 0 \tag{30c}$$

$$\Theta_\eta(\eta = 0^-)/\Theta_\eta(\eta = 0^+) = k/k_s \quad \text{at} \quad \eta = 0 \tag{30d}$$

$$\Theta_\eta = 0 \quad \text{at} \quad \xi > 0,\ \eta = -1/\xi\sqrt{2} \tag{30d}$$

The relationships 29 and 30 give the dimensionless parameters governing the thermal phenomena. They are

$$\xi \quad \eta, \quad \nu/\alpha = \text{Pr}, \quad \nu/\alpha_s, \quad k/k_s$$

The temperature field over the ξ, η domain depends on the gas properties through its Prandtl number, and on the yarn thermodynamical properties by ν/α_s and k/k_s. Usually the melt-spinning process takes place in the air, for which a Prandtl number of 0.72 has been assumed, but the fourth and fifth parameters, ν/α_s and k/k_s must be determined from the polymer characteristics. They may affect the axial temperature distribution along the yarn. As a result, the thermal quantities and the Nusselt number characterizing the heat transfer become functions of ξ.

The thermal boundary-layer displacement thickness for a cylinder is defined as follows:

$$\pi(\delta_T^* + a)^2 - \pi a^2 = \int_0^\infty \frac{u}{u_e}\cdot\frac{T - T_{wo}}{T_e - T_{wo}}\,2\pi r\,dr$$

Using the dimensionless variables gives the following:

$$\left(\frac{\delta_T^*}{a} + 1\right)^2 - 1 = 2\xi\int_0^\infty f_\eta\cdot(1 - \Theta)\,d\eta \tag{31}$$

The following relation can be derived from the heat transfer coefficient definition.

$$\text{Nu}_a\cdot\xi = \text{Nu}_x\cdot 1/\sqrt{\text{Re}_x} = 1/\sqrt{2}\cdot\Theta_\eta(\xi, \eta = 0)/\Theta(\xi, \eta = 0) \tag{32}$$

The temperature along the yarn axis can be computed as a function of x through ξ:

$$\Theta_{\text{axis}} = \Theta(\xi, \eta = -1/\xi\sqrt{2}) \tag{33}$$

The axial gradient, which indicates the cooling rate experienced by the yarn during its motion away from the spinneret, is given by the following:

$$\frac{\partial T}{\partial x} = \frac{\Delta T_{wo}}{2a}\cdot\text{Re}_x^{-1/2}\cdot\Theta_\xi \Rightarrow \frac{\partial T}{\partial x}\cdot\frac{a}{\Delta T_{wo}}\cdot\text{Re}_x^{1/2} = \frac{\Theta_\xi}{2} \tag{34}$$

Solving the laminar boundary-layer equations

Numerical scheme

The boundary-layer equations are parabolic. The ξ coordinate is the marching direction, along which the Crank–Nicholson scheme is applied. The nodes are located in ξ^n and ξ^{n+1}; whereas the equation is written at $\xi^{n+1/2}$. The following discretization is introduced in the equations.

$$\xi \leftarrow \xi^{n+1/2} = \frac{\xi^{n+1} + \xi^n}{2} \tag{35}$$

$$f \leftarrow f^{n+1/2} = \frac{f^{n+1} + f^n}{2} \tag{36}$$

$$\frac{\partial f}{\partial \xi} \leftarrow \left(\frac{\partial f}{\partial \xi}\right)^{n+1/2} = \frac{f^{n+1} - f^n}{\xi^{n+1} - \xi^n} \tag{37}$$

Mesh generation

Algebraic meshes are used. For the ξ-direction, a stretching is needed close to the origin to capture the beginning of the growth of the boundary layer. The following shape function is used (following Thompson et al. (1985)):

$$S_1(z) = 1 + \tanh[c(z - 0.5)]/\tanh(c/2) \tag{38}$$

where c is a parameter governing the stretching intensity. The same function is used to generate the η-mesh of the momentum computation, where the stretching is needed close to the wall. For the η-mesh of the thermal computation, the stretching is

centered around the air–yarn interface by using the following formula:

$$S_2(z) = \alpha_m \cdot (1 + \sinh[\beta_m(z - A)]/\sinh(\beta_m A)) \quad (39)$$

from Hoffmann (1989), where A is defined as follows:

$$A = 1/2\beta_m \ln([1 + (e^{\beta_m} - 1)\alpha_m]/[1(\bar{e}^{\beta_m} - 1)\alpha_m]) \quad (40)$$

α_m governs the position of the stretching center in [0, 1] and β_m its intensity. The last of the boundary conditions, Equation 29, has $\eta \to \infty$ as $\xi \to 0$. We truncated the domain at $\eta = -5$. It is observed that the solution does not change significantly below $\eta = -2$. The computations are carried out between the hyperbola and a free-stream limit obtained when $\partial f/\partial \eta$ is below a given value.

Results

Wind-tunnel case

Results for the wind-tunnel case are shown in Figure 3. At the wall ($\eta = 0$) the velocity is zero, and tends to unity in the free stream. This solution, previously obtained by Sawchuk and Zamir (1992), corresponds to a semi- infinite cylinder mounted in a wind tunnel. The wind-tunnel computation is the test case

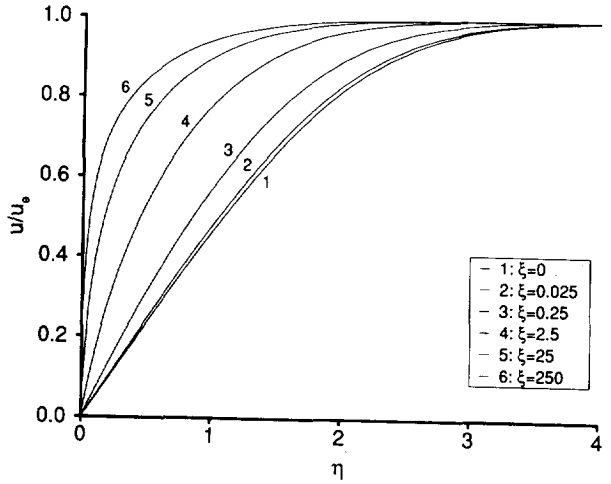

Figure 3 u-velocity profile for the wind-tunnel case

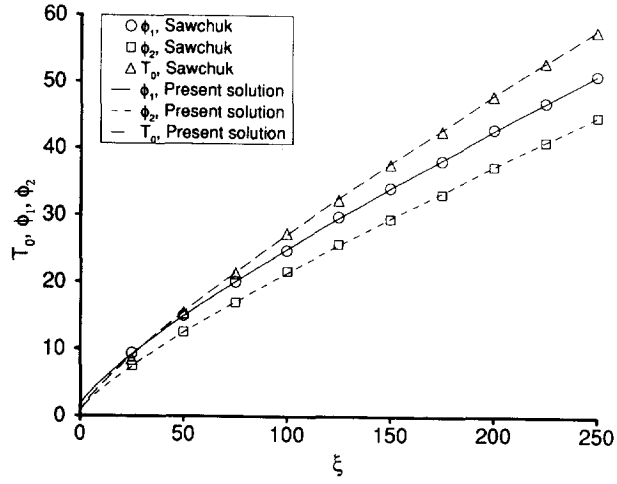

Figure 4 Comparison with Sawchuk's and Zamin's (1992) results: ϕ_1, ϕ_2 and T_0

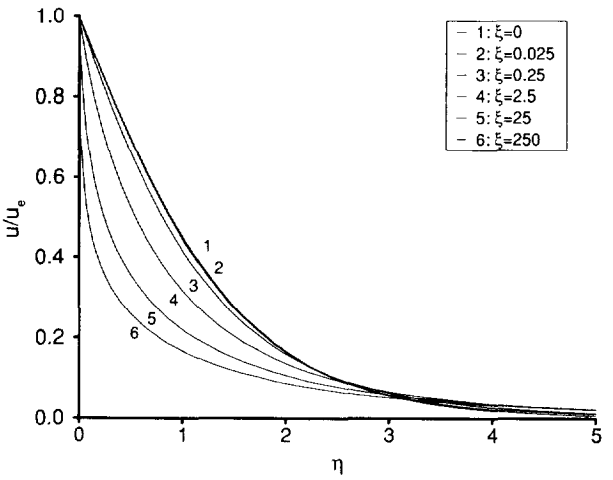

Figure 5 u-velocity profile for the spinneret case

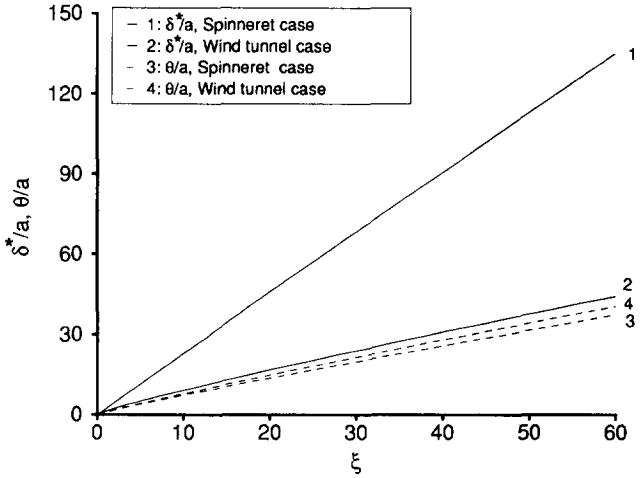

Figure 6 Boundary-layer displacement thickness, momentum displacement thickness

of the numerical code, and is compared with Sawchuk's and Zamir's results in Figure 4, in terms of ϕ_1, ϕ_2, and T_o defined in his paper.

Spinneret case

In the second case, the continuous body is leaving a spinneret. The corresponding u-velocity profiles are shown in Figure 5.

Comparison

A significant difference is that the solution for the spinneret case remains closer to the flat plate solution for higher values of ξ than for the wind-tunnel case. As shown in Figure 5, there is no major difference between the flat plate solution and the curves obtained for $\xi = 0$, 0.025, 0.25 for the spinneret case, whereas the curve $\xi = 0.25$ of the wind-tunnel case is already significantly different.

Figure 6 shows the boundary-layer displacement thickness δ^*/a and the momentum thickness θ/a plotted against ξ for both cases. The boundary layer is thicker in the case of a yarn leaving a spinneret. The momentum thickness shows the opposite behavior. The momentum thickness is smaller for the spinneret case, although its displacement thickness is larger. This is because the velocity profiles are steeper near the wall

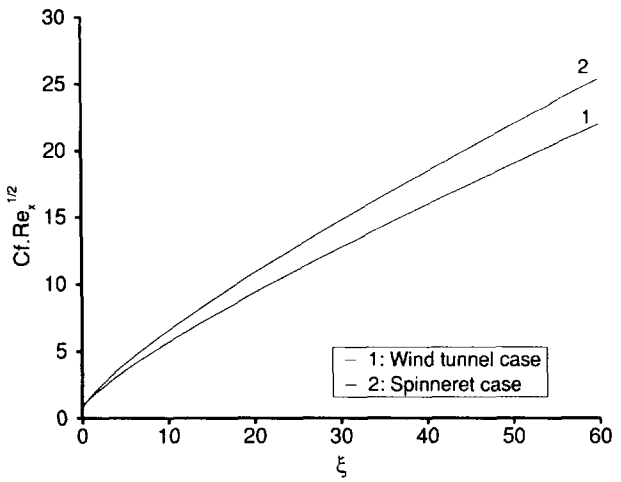

Figure 7 Friction coefficient

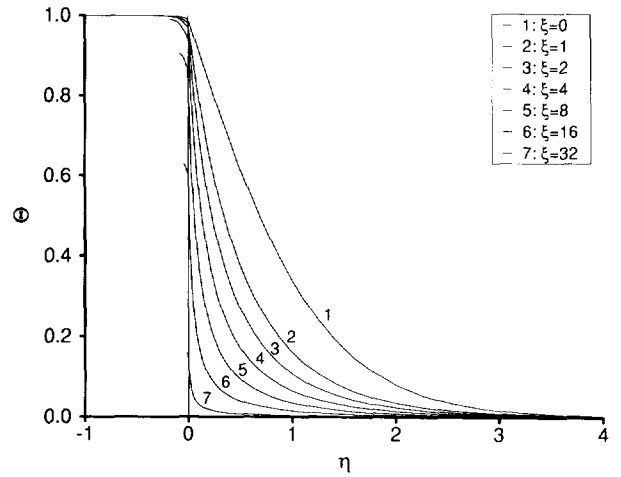

Figure 8 Temperature profiles in the air ($\eta > 0$) and in the yarn ($\eta < 0$), for $v/\alpha_s = 80$, 100, 120, and 140, $k/k_s = 0.1$, Pr = 0.72

and tend more slowly to the free-stream velocity. Figure 7 gives the friction coefficient. Again, the difference between the two curves reveals a significant theoretical difference between the two cases. This would imply that results of experimental wind-tunnel simulations should not be directly applied to fiber spinning, particularly in the laminar region.

Thermal boundary-layer

The thermal computations are carried out for $k/k_s = 0.1$ and four values of v/α_s: 80, 100, 120, and 140. They are typical values of polymers used in the melt-spinning process. The results of the thermal computation are shown in Figure 8. The temperature profiles are given in the yarn ($\eta < 0$) for different values of ξ. The dimensionless temperature decreases from 1 at the exit of the spinneret ($\xi = 0$, $\eta = 0$) to 0 at infinity ($\eta = +\infty$). The temperature in the center of the yarn (i.e., the leftmost point of each curve of the last plot) is given in Figure 9 as a function of ξ. The cylinder keeps its initial temperature till $\xi \approx 5$, and then its temperature decreases. The thermal exchange is characterized in Figure 10 where $Nu_a \cdot \xi$ is plotted versus ξ. Figure 11 shows the relationship between the Stanton number and the friction coefficient. The axes are $St \cdot Re_x^{1/2}$

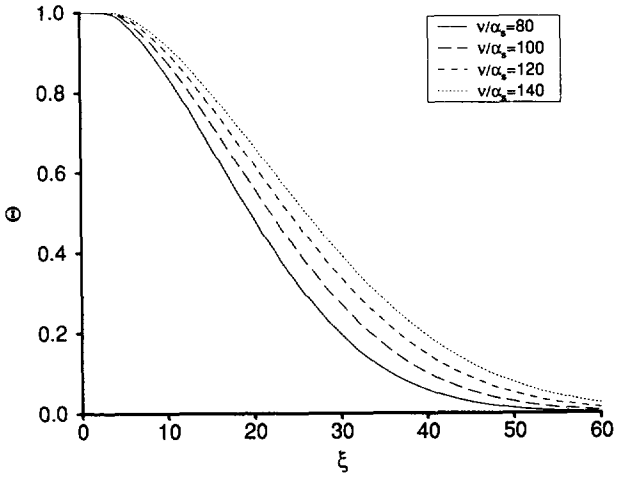

Figure 9 Temperature along the yarn axis, for $v/\alpha_s = 80$, 100, 120, and 140, $k/k_s = 0.1$, Pr = 0.72

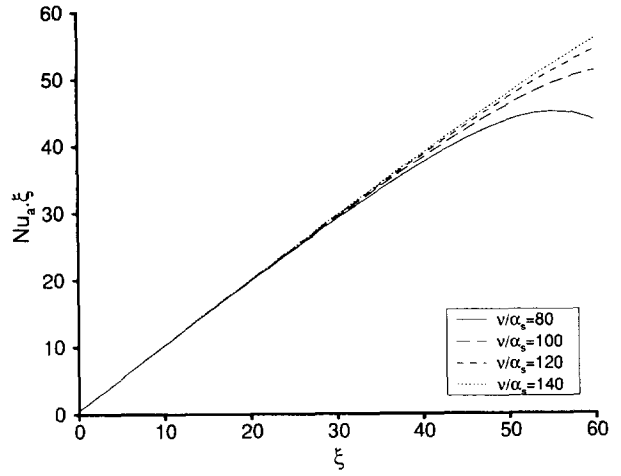

Figure 10 Nusselt number along the yarn, for $v/\alpha_s = 80$, 100, 120, and 140, $k/k_s = 0,1$, Pr = 0.72

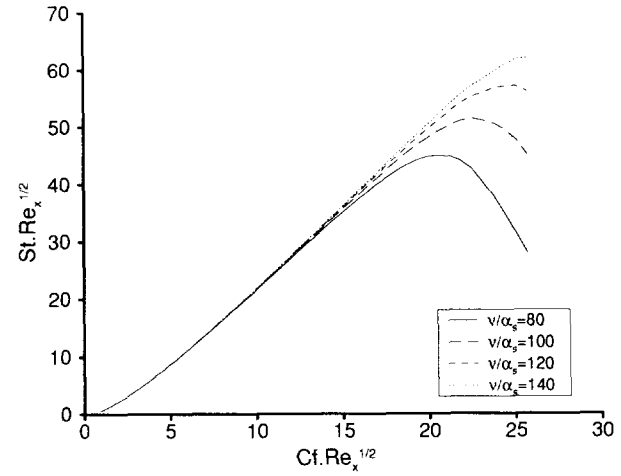

Figure 11 Comparison Stanton number—friction coefficient, along the yarn, for $v/\alpha_s = 80$, 100, 120, and 140, $k/k_s = 0.1$, Pr = 0.72

versus $C_f \cdot \mathrm{Re}_x^{1/2}$. In the case of a thermal analogy, the Stanton number and the friction coefficient would be proportional, so the graph would be a straight line crossing the origin. This is not the case: there is obviously a relationship between them, but it is not as simple as a proportionality factor. This conclusion is not changed by the presence of $\mathrm{Re}_x^{1/2}$, because it appears on both axes. Removing it would require given values of air viscosity and yarn velocity, yielding a result that would no longer be universal.

Conclusion

The theory developed in this paper is based on previous work giving the quasi-similar solution of the laminar axisymmetric boundary layer in the wind-tunnel case. Here we give the solution for a continuous moving surface and present the same approach for the thermal boundary layer.

The comparison between the momentum boundary layer along a semi-infinite body and along a continuous moving body, yields the conclusion that the growth of the boundary layer is strongly affected by the boundary condition type. It is, therefore, to be expected that an experimental investigation of the fiber spinning in a wind tunnel will not give quantitatively correct results.

The theoretical analysis of the thermal boundary layer provides the governing parameters of the laminar solution. The numerical solution gives interesting results, such as the temperature distribution along the yarn centerline, and demonstrates that there is no thermal analogy between the skin friction and the heat transfer.

Acknowledgment

This work was partially supported by Rhône Poulenc Fibres (France). We are grateful to J.-M. Buchlin for fruitful discussions.

References

Glauert, M. B. and Lighthill, M. J. 1955. The axisymmetric boundary layer on a long thin cylinder. *Proc. R. Soc. Lond.* [*Math. Phys. Sci.*], **230**, 188–203

Hoffman, K. A. 1989. *Computational Fluid Dynamics for Engineers.* University of Texas Press, Austin, TX, 250–258

Jaffe, N. A. and Okamura, T. T. 1968. The transverse curvature effect on the incompressible laminar boundary layer for longitudinal flow over a cylinder. *Z. Angawandte Mathematik Physik*, **19**, 564–574 **19**, 564–574

Kao, K.-H. and Chow, C.-Y. 1991. Stability of the boundary layer on a spinning semi-infinite circular cylinder. *J. Spacecraft*, **28**, 284–291

Sakiadis, B. C. 1961a. Boundary-layer behavior on continuous solid surfaces: I. Boundary-layer equations for two-dimensional and axisymmetric flow. *AIChE J.*, **7**, 26–28

Sakiadis, B. C. 1961b. Boundary-layer behavior on continuous solid surfaces: II. The boundary-layer on a continuous flat surface. *AIChE J.*, **7**, 221–225

Sakiadis, B. C. 1961c. Boundary-layer behavior on continuous solid surfaces: III. The boundary-layer on a continuous cylindrical surface. *AIChE J.*, **7**, 467–472

Sawchuk, S. P. and Zamir, M. 1992. Boundary layer on a circular cylinder in axial flow. *Int. J. Heat Fluid Flow*, **13**, 184–188

Seban, R. A. and Bond, R. 1951. Skin-friction and heat transfer characteristics of a laminar boundary layer in axial compressible flow. *J. Aeronaut. Sci.*, **18**, 671–675

Thompson, J. F., Warsi, Z. U. A. and Wayne Mastin, C. 1985. *Numerical Grid Generation, Foundation and Applications.* Elsevier, New York